Computational studies of the glass-forming ability of model bulk metallic glasses

Kai Zhang (张凯),[1,2] Minglei Wang (王明磊),[1,2] Stefanos Papanikolaou,[1,2,3]
Yanhui Liu (柳延辉),[1,2] Jan Schroers,[1,2] Mark D. Shattuck,[1,4] and Corey S. O'Hern[1,2,3,5]
[1]*Department of Mechanical Engineering and Materials Science, Yale University, New Haven, Connecticut 06520, USA*
[2]*Center for Research on Interface Structures and Phenomena, Yale University, New Haven, Connecticut 06520, USA*
[3]*Department of Physics, Yale University, New Haven, Connecticut 06520, USA*
[4]*Department of Physics and Benjamin Levich Institute, The City College of the City University of New York, New York, New York 10031, USA*
[5]*Department of Applied Physics, Yale University, New Haven, Connecticut 06520, USA*

(Received 1 May 2013; accepted 4 September 2013; published online 23 September 2013)

Bulk metallic glasses (BMGs) are produced by rapidly thermally quenching supercooled liquid metal alloys below the glass transition temperature at rates much faster than the critical cooling rate R_c below which crystallization occurs. The glass-forming ability of BMGs increases with decreasing R_c, and thus good glass-formers possess small values of R_c. We perform molecular dynamics simulations of binary Lennard-Jones (LJ) mixtures to quantify how key parameters, such as the stoichiometry, particle size difference, attraction strength, and heat of mixing, influence the glass-formability of model BMGs. For binary LJ mixtures, we find that the best glass-forming mixtures possess atomic size ratios (small to large) less than 0.92 and stoichiometries near 50:50 by number. In addition, weaker attractive interactions between the smaller atoms facilitate glass formation, whereas negative heats of mixing (in the experimentally relevant regime) do not change R_c significantly. These results are tempered by the fact that the slowest cooling rates achieved in our simulations correspond to $\sim 10^{11}$ K/s, which is several orders of magnitude higher than R_c for typical BMGs. Despite this, our studies represent a first step in the development of computational methods for quantitatively predicting glass-formability. [http://dx.doi.org/10.1063/1.4821637]

I. INTRODUCTION

When supercooled liquids are rapidly quenched at rates R exceeding a critical value R_c, crystallization is avoided, and systems form disordered solids such as bulk metallic glasses (BMGs). BMGs possess high mechanical strength and can be processed so that they display plastic,[1] not brittle, response to applied deformations, which makes them desirable materials for a variety of industrial and engineering applications.[2] Avoiding crystallization in pure metals requires enormously large cooling rates in excess of 10^{12} K/s. However, bulk metallic glass-forming alloys have been developed for which the critical cooling rate is more than nine orders of magnitude lower, in the range $1 < R_c < 10^3$ K/s. Understanding the important physical quantities that determine the glass-forming ability (GFA) of multi-component alloys will allow us to develop even stronger and less costly bulk metallic glasses.

Prior research suggests that multi-component metallic alloys with $T_g/T_m \gtrsim 0.67$ form BMGs, where T_g and T_m are the glass transition and melting temperature, respectively.[3] In addition, Inoue[2] has emphasized three guidelines for enabling BMG formation, rather than crystallization: (1) atomic size ratios (small relative to large) of $\alpha < 0.89$ for at least two constituents of the alloy; (2) large negative heats of mixing;[4] and (3) several atomic components. In Fig. 1, we show the distributions of the atomic size ratios and heats of mixing for common binary and ternary bulk metallic glass-forming alloys.[5] For binary systems, the most probable atomic size ratio is $\alpha \approx 0.8$ and heat of mixing is negative and roughly 6%–7% of the average cohesive energy.

However, beyond these heuristic guidelines, there is no quantitative and predictive understanding of the glass-forming ability in multi-component alloys. (Note that there have been previous measurements of the critical cooling rate in binary hard-sphere systems.[6,7]) For model BMG-forming systems with attractive interactions, we do not know the dependence of the critical cooling rate on the stoichiometry, size ratios, and heats of mixing of the constituent atomic species. For example, can multi-component systems with large negative heats of mixing, but smaller atomic size mismatches, possess the same glass-forming ability as systems with small negative heats of mixing but larger atomic size mismatches?

To answer these questions, we perform molecular dynamics (MD) simulations of model glass-forming systems, binary Lennard-Jones (LJ) mixtures of spherical particles, to measure the critical cooling rate as a function of the size ratio, number fraction, and interaction energy of the two particle species. We find several important results. First, the critical cooling rate decreases exponentially with the particle size ratio, $R_c \sim \exp[-C(1-\alpha)^3]$, where C depends on the number fraction of small and large particles. At a given size ratio $\alpha < 1$, the minimum critical cooling rate occurs at

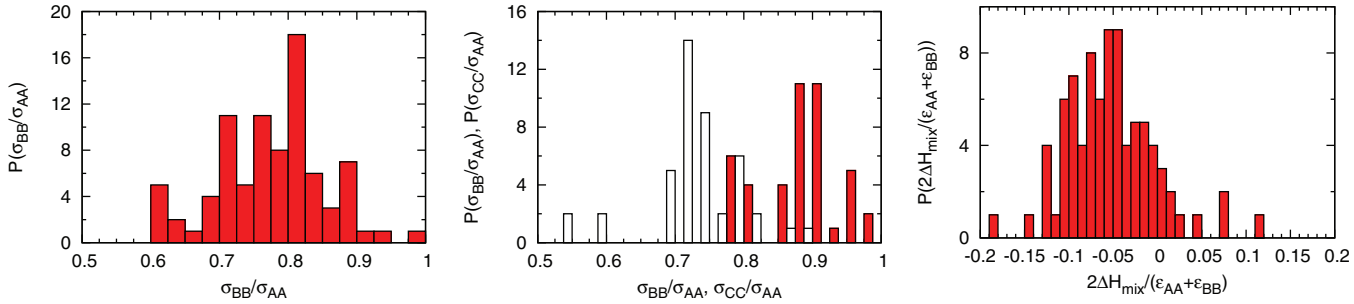

FIG. 1. (Left) Probability distribution $P(\sigma_{BB}/\sigma_{AA})$ of atomic size ratios (with $\sigma_{BB} < \sigma_{AA}$) in binary bulk metallic glasses.[5] (Middle) Probability distributions of atomic size ratios $P(\sigma_{BB}/\sigma_{AA})$ (shaded) and $P(\sigma_{CC}/\sigma_{AA})$ (white) (with $\sigma_{CC} < \sigma_{BB} < \sigma_{AA}$) in ternary BMGs.[5] (Right) Probability distribution of the heats of mixing $\Delta H_{\rm mix}$ relative to the average cohesive energy $(\epsilon_{AA} + \epsilon_{BB})/2$ in binary BMGs.[4,5]

the number fraction corresponding to equal volumes of the large and small particles. In addition, we find that at fixed number fraction and size ratio, the critical cooling rate decreases strongly with decreasing cohesive energy ratio of the small particles relative to the large ones, $\epsilon_{BB}/\epsilon_{AA}$. In contrast, variations of the heat of mixing of the two species in the experimentally accessible range do not affect R_c significantly. Thus, we have quantified several design principles for improving glass formation in binary mixtures. These results are tempered by the fact that the cooling rates achieved in our simulations are several orders of magnitude larger than the critical cooling rates of typical BMGs, and thus the glass-forming abilities of the model systems considered here are much poorer than those realized in experiments.

II. SIMULATION METHODS

We perform constant number, volume, and temperature (NVT) MD simulations of binary LJ mixtures of $N = N_A + N_B$ spherical particles with the same mass m, but different diameters σ_{AA} and σ_{BB}, in periodic cubic cells with volume $V = L^3$. The particles interact pairwise via the LJ potential

$$u(r_{ij}) = 4\epsilon_{ij}\left[\left(\frac{\sigma_{ij}}{r_{ij}}\right)^{12} - \left(\frac{\sigma_{ij}}{r_{ij}}\right)^{6}\right], \qquad (1)$$

where $i, j \in \{A, B\}$, B indicates the smaller particle, $\sigma_{ij} = (\sigma_{ii} + \sigma_{jj})/2$ unless otherwise specified, and ϵ_{AA} and ϵ_{BB} represent the cohesive energies for the A and B particles, respectively. We quantify the heat of mixing using $\Delta H_{\rm mix} = (\epsilon_{AA} + \epsilon_{BB})/2 - \epsilon_{AB}$. We employ the shifted-force version of the LJ potential (Eq. (1)) so that the pair potential and force vanish for separations beyond the cutoff distance $r_{\rm cut} = 3.5\sigma_{ij}$.[17] Energies, lengths, timescales, and temperatures are given in units of ϵ_{AA}, σ_{AA}, $\sigma_{AA}\sqrt{m/\epsilon_{AA}}$, and ϵ_{AA}/k_B, respectively, where the Boltzmann constant k_B is set to unity.

Note that the specific choice of the interaction parameters for the LJ potential in Eq. (1), $\epsilon_{AA} = 1.0$, $\epsilon_{AB} = 1.5$, $\epsilon_{BB} = 0.5$, $\sigma_{AA} = 1.0$, $\sigma_{AB} = 0.8$, and $\sigma_{BB} = 0.88$ with $f_B = N_B/N = 0.2$, gives the Kob-Andersen model for glass-forming liquids. This and similar models have been employed extensively over the past 20 years to study the super-Arrhenius temperature dependence of the structural and stress relaxation times,[8–10] aging[11] and rejuvenation,[12] and cooling rate dependence of thermodynamic properties[13] near the glass transition. The Kob-Andersen model has been also used to identify soft spots[14] and dynamical heterogeneities[15] in supercooled liquids and mimic the vapor deposition process to produce extremely metastable glasses.[16]

In our studies, we varied the glass-forming ability of binary LJ mixtures by tuning the number fraction f_B, particle size ratio $\alpha = \sigma_{BB}/\sigma_{AA}$, relative cohesive energy $\epsilon_{BB}/\epsilon_{AA}$, and heat of mixing $\Delta H_{\rm mix}$. In most cases, we fixed the packing fraction $\phi = N\sigma_{AA}^3(1 + f_B(\alpha^3 - 1))\pi/6V = 0.524$ (with the minimum in the LJ potential at $r_{\rm min} = 2^{1/6}\sigma_{ij}$) at a typical value for binary BMGs,[5] which corresponds to number density $\rho \equiv N\sigma_{AA}^3/V = 1$ for monodisperse and $\rho = 1/(1 + f_B(\alpha^3 - 1))$ for bidisperse systems. We only show results for $0.92 \le \alpha \le 1$ for which solid solutions with face-centered cubic (FCC) crystal structures are in the equilibrium phase.[18]

We initialize the systems at high temperature $T_0 = 2.0$, using the Nosé-Hoover thermostat,[19,20] and then thermally quench the systems exponentially, $T(t) = T_0 e^{-Rt}$, from T_0 to $T_f = 10^{-2}$ at various rates R over four orders of magnitude at constant volume. (In Appendix A, we show that our results are not sensitive to the choice of the thermostat and the form of the cooling schedule. In addition, we show in Appendix C that we find qualitatively similar results for cooling at constant pressure versus constant volume.)

For typical BMGs, $\sigma_{AA} \sim 3 \times 10^{-10}$ m, $\epsilon_{AA}/k_B \sim 10^3$ K, and the molar mass $M \sim 10^{-1}$ kg/mol,[21] and thus the time unit in our simulations corresponds to roughly $\sigma_{AA}\sqrt{m/\epsilon_{AA}} \sim 10$ ps. A cooling rate $R = 1$ in dimensionless units corresponds to an extremely rapid thermal quench, 10^{15} K/s, in experimental BMGs. Thus, the slowest cooling rate studied in our MD simulations corresponds to 10^{11} K/s, which is comparable to rates used to prepare thin films[16] not bulk samples.

While MD simulations of metal alloys are not currently able to achieve sufficiently slow cooling rates to match those employed in bulk samples, there are a number of fundamental questions about glass-forming ability that can be addressed by MD simulations. First, note that there is a trade-off between the intrinsic glass-forming ability of a system and typical cooling rates employed to study glass formation, i.e., poor glass formers require faster cooling rates to achieve amorphous states. Here, we deliberately focus on weakly polydisperse Lennard-Jones systems, which are extremely poor glass formers, so that we can tune cooling rates over a

computationally accessible range where we can achieve both crystalline and amorphous systems. For more strongly polydisperse systems, only glassy states are attainable at cooling rates accessible to MD simulations. We are interested in understanding the physical mechanisms that distinguish a poor versus a good glass-forming material, and thus it is important to study a broad range of GFAs and critical cooling rates.

Following the thermal quenches to T_f, we characterize the structural properties of the system by measuring several quantities: (1) the local and global bond orientational order parameters[22–26]

$$Q_6^l = \frac{1}{N}\sum_{i=1}^{N}\left(\frac{4\pi}{13}\sum_{m=-6}^{6}\left|\frac{1}{n_i}\sum_{j=1}^{n_i}Y_6^m(\theta_{ij},\phi_{ij})\right|^2\right)^{1/2}, \quad (2)$$

$$Q_6^g = \left(\frac{4\pi}{13}\sum_{m=-6}^{6}\left|\frac{1}{N}\sum_{i=1}^{N}\frac{1}{n_i}\sum_{j=1}^{n_i}Y_6^m(\theta_{ij},\phi_{ij})\right|^2\right)^{1/2}, \quad (3)$$

where θ_{ij} and ϕ_{ij} are the axial and polar angles between each particle i and its neighbors j, Y_6^m are spherical harmonics of degree 6 and order m, and n_i is the number of nearest neighbors of particle i within a cutoff distance of $1.5\sigma_{ij}$; (2) local bond orientational order position correlation function

$$G_6(r) = \frac{4\pi}{13}\sum_{m=-6}^{6}\frac{\left|\sum_i\sum_{j\neq i}q_{6m}(\vec{r}_i)q_{6m}(\vec{r}_j)\delta(\vec{r}-\vec{r}_{ij})\right|}{g(r)}, \quad (4)$$

where $g(r) = \sum_i\sum_{j\neq i}\delta(\vec{r}-\vec{r}_{ij})$ is the radial distribution function and $q_{6m}(\vec{r}_i) = n_i^{-1}\sum_{j=1}^{n_i}Y_6^m(\theta_{ij},\phi_{ij})$; and (3) the crystal domain size. These structural quantities are averaged over at least 96 independent quenching trajectories. (In Appendix B, we compare the results for the critical quench rate using these measures of structural order.) We consider system sizes from $N = 500$ to 8788 particles.

III. RESULTS

In this section, we characterize the structural properties of LJ systems thermally quenched to temperature T_f as a function of the cooling rate R at constant volume. In the right inset of the left panel of Fig. 2, we show the distribution $P(Q_6^l)$ of the local bond orientational order parameter Q_6^l for monodisperse LJ systems with $N = 1372$ particles. For fast cooling rates, e.g., $R = 0.02$, most of the quenched systems are structurally disordered, and $P(Q_6^l)$ possesses a strong peak at small $Q_6^l \sim 0.41$. In contrast, for slow cooling rates, e.g., $R = 0.005$, most of the quenched systems are ordered, and $P(Q_6^l)$ possesses a strong peak at a larger value of $Q_6^l \sim 0.51$. For intermediate cooling rates, the distribution $P(Q_6^l)$ becomes strongly bimodal, which indicates that the systems possess disordered as well as ordered regions. In the main panel of Fig. 2 (left), we show the median $\overline{Q}_6^l$ versus the logarithm of the cooling rate R for several system sizes. For each system size, $\overline{Q}_6^l$ first increases modestly with decreasing cooling rate, followed by a rapid increase at intermediate rates, and then it plateaus with further decreases. We define the critical cooling rate, R_c, as the rate at which the median local bond orientational order parameter crosses the threshold value $\overline{Q}_6^l = Q_0 = 0.43$. We chose the threshold Q_0 (for both monodisperse and bidisperse systems) for several reasons: (1) Q_0 captures the steep rise in $\overline{Q}_6^l$ with decreasing cooling rate, (2) Q_0 is in the region of Q_6^l between the two peaks in $P(Q_6^l)$ that occur at intermediate cooling rates (right inset of left panel of Fig. 2), and (3) Q_0 is a value for which $\overline{Q}_6^l(R)$ becomes system size independent for intermediate and fast cooling rates.

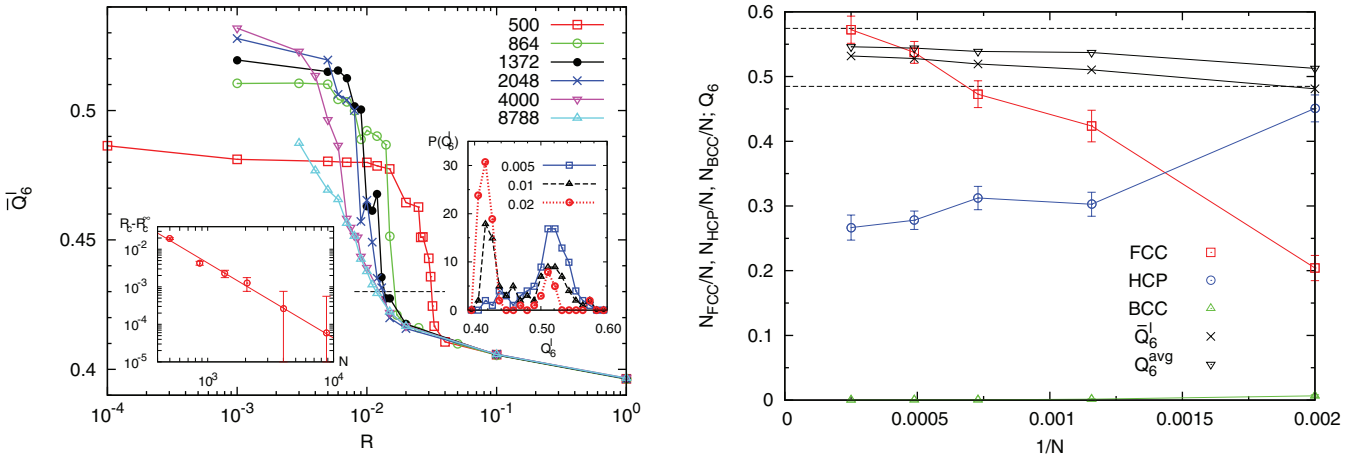

FIG. 2. (Left) Median local bond orientational order parameter $\overline{Q}_6^l$ for monodisperse Lennard-Jones (LJ) systems following thermal quenches to $T_f = 0.01$ over a range of cooling rates R for system sizes $N = 500$, 864, 1372, 2048, 4000, and 8788. The critical cooling rate R_c (defined as the rate at which $\overline{Q}_6^l = 0.43$ (dashed line)) approaches its large-N limit, R_c^∞, as a power-law $R_c - R_c^\infty \sim 1/N^2$ (left inset). (Right inset) The probability distribution $P(Q_6^l)$ for monodisperse LJ systems with $N = 1372$ following quenches to $T_f = 0.01$ for cooling rates $R = 0.02$ (○), 0.01 (△), and 0.005 (□). (Right) Fraction of particles that occur in HCP (○), FCC (□), and BCC (△) crystal clusters as a function of $1/N$ for monodisperse LJ systems following a quench to T_f at cooling rate $R = 10^{-3} < R_c$. At this rate, $\overline{Q}_6^l$ (×) agrees with the value (▽) obtained by averaging $Q_6^l = 0.575$ for FCC and $Q_6^l = 0.485$ for HCP (dashed lines) weighted by the fraction of particles in FCC and HCP clusters in each sample. In both panels, the systems were cooled at constant volume with $\rho = 1$.

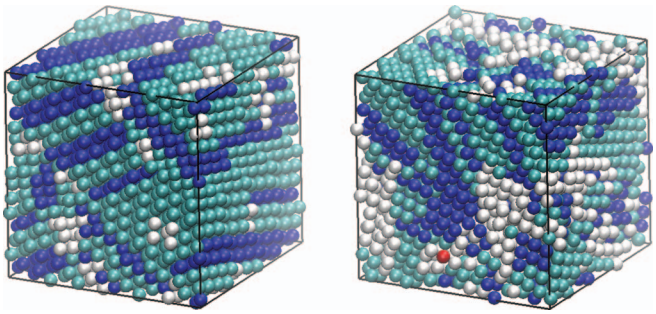

FIG. 3. Crystalline clusters obtained in monodisperse LJ systems with $N = 4000$ following thermal quenches to $T_f = 0.01$ at cooling rates $R = 10^{-3}$ (left) and 10^{-2} (right) at constant volume with $\rho = 1$. Particles are colored according to whether they belong to FCC (cyan), HCP (blue), BCC (red), or non-crystalline (white) domains at T_f.

Note that the distribution of the global bond orientational order parameter $P(Q_6^g)$ also becomes bimodal and the median $\overline{Q}_6^g$ increases rapidly with decreasing cooling rate. (See Appendix B.) However, the global bond orientational order parameter quantifies crystallization of the *entire* system, which is influenced more by the slow dynamics of crystal growth, rather than the initial nucleation of crystalline domains.

The value of the bond orientational order parameter depends on the crystal structure that forms during the thermal quenching process. Thus, we employed a crystal analysis algorithm to identify the crystalline clusters (FCC, hexagonal close packed (HCP),[27] or body-centered-cubic (BCC)) for cooling rates $R \lesssim R_c$. For example, $Q_6^l \approx 0.575$ for an ideal FCC structure, whereas it is ≈0.485 for an ideal HCP structure. This difference explains the increase in $\overline{Q}_6^l$ for $R \ll R_c$ as N increases in the main panel of Fig. 2 (left). In Fig. 2 (right), we show that small systems ($N \leq 500$) mainly crystallize to HCP structures,[28,42] while larger systems crystallize predominantly to FCC structures. For low cooling rates, e.g., $R = 10^{-3}$, the median local bond orientational order parameter $\overline{Q}_6^l$ can be obtained by averaging the Q_6^l values for FCC and HCP structures weighted by the fraction of particles in FCC and HCP clusters in each sample. (See Fig. 2 (right).) We show snapshots of the thermally quenched structures for monodisperse LJ systems using two cooling rates in Fig. 3 with FCC, BCC, HCP, and non-crystalline regions shaded in different colors.

We show the system-size dependence of the critical cooling rate R_c for monodisperse LJ systems in the left inset to the left panel of Fig. 2. We find that R_c decreases with increasing system size and approaches its large-N limit, $R_c^\infty \approx 0.01$, as a power law $R_c - R_c^\infty \sim 1/N^2$. It is interesting that the approach to R_c^∞ scales as $1/N^2$, which is faster than the $1/N$ scaling typical for first-order transitions. In contrast to hard-sphere systems,[29] crystallization in monodisperse LJ systems is more difficult at large N. In small monodisperse LJ systems ($N \leq 500$), the critical nucleus is sufficiently large that it interacts with its periodic images,[30,31] which reduces the interfacial energy of crystal nuclei and enhances the formation of single crystals.

We now focus on binary LJ systems at fixed $N = 1372$ and cohesive energy ratio $\epsilon_{BB}/\epsilon_{AA} = 1$ and study the glass-forming ability as a function of the size ratio α and number fraction f_B. For $\alpha \lesssim 1$, the smallest $R_c(\alpha, f_B)$ (i.e., best glass-former) is obtained in systems with approximately equal numbers of A and B particles, $f_B^* \approx 0.5$, as shown in Fig. 4 (left). As α decreases, the minimum in $R_c(\alpha, f_B)$ deviates from $f_B^* \approx 0.5$ and follows $f_B^* = 1/(1+\alpha^3)$ for which the A and B particles occupy the same volume (reaching $f_B^* \approx 0.56$ at $\alpha = 0.92$). As shown in Fig. 4 (right), at each f_B, R_c decreases exponentially with decreasing size ratio, $R_c(\alpha, f_B) = R_c(1, f_B)\exp[-C(f_B)(1-\alpha)^3]$. This result implies that R_c drops from 10^{-2} to 10^{-11}–10^{-25} for binary systems of composition $f_B = 0.2$–0.8 with size ratio $\alpha = 0.8$ (the most common size ratio in binary bulk metallic glass formers), which is 9–23 orders slower than R_c at $\alpha = 1$. We also note that for a given cooling rate R, the glass-forming regime, i.e., the range of number fractions for which $R > R_c$, expands with decreasing α.

For the results presented so far, we set the cohesive energy ratio $\epsilon_{BB}/\epsilon_{AA} = 1$. However, as shown in the inset to Fig. 5, the cohesive energy between like species is different

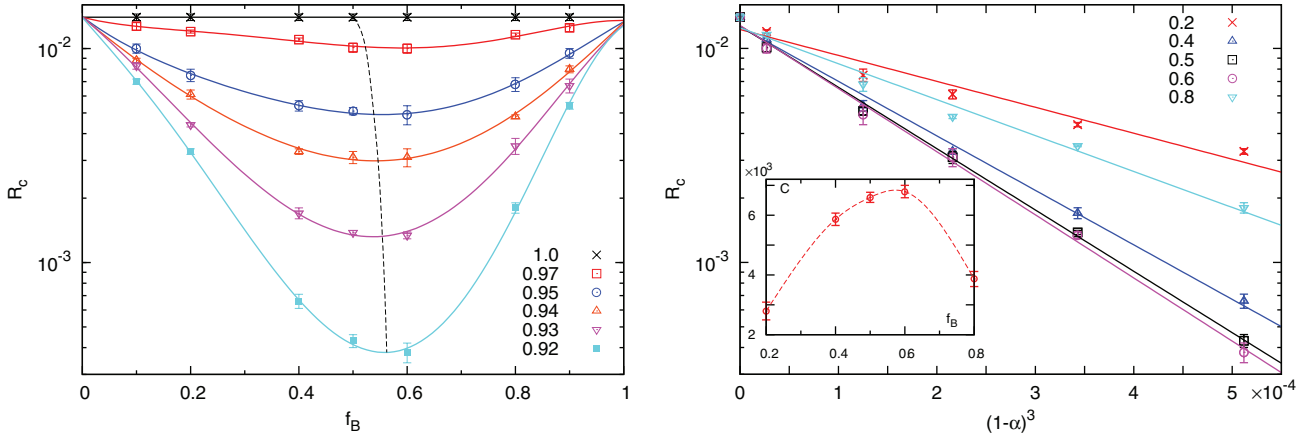

FIG. 4. (Left) Critical cooling rate R_c for binary LJ mixtures with $N = 1372$ as a function of the number fraction f_B for several particle size ratios $\alpha = 1.0$, 0.97, 0.95, 0.94, 0.93, and 0.92. The solid lines are sixth-order least-square fits to the data for R_c. The dashed line connects the number fractions $f_B^* = 1/(1+\alpha^3)$ at which the A and B particles occupy the same volume. (right) R_c versus $(1-\alpha)^3$ for binary LJ mixtures with $f_B = 0.2$, 0.4, 0.5, 0.6, and 0.8. The error bars for R_c are determined by the cooling rate increment $\Delta R = 10^{-3}$. The inset shows the coefficient $C(f_B)$ of the exponential decay of $R_c \sim \exp[-C(1-\alpha)^3]$.

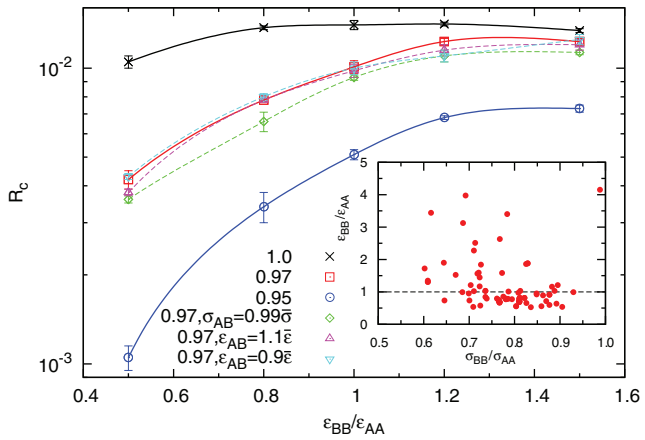

FIG. 5. Critical cooling rate R_c as a function of the cohesive energy ratio $\epsilon_{BB}/\epsilon_{AA}$ for binary LJ mixtures with $N = 1372$, number fraction $f_B = 0.5$, and size ratios $\alpha = 1.0$, 0.97, and 0.95. The solid lines indicate results for the mixing rule $\sigma_{AB} = \bar{\sigma} \equiv (\sigma_{AA} + \sigma_{BB})/2$ and $\epsilon_{AB} = \bar{\epsilon} \equiv (\epsilon_{AA} + \epsilon_{BB})/2$. The dashed lines indicate results for positive ($\epsilon_{AB} = 0.9\bar{\epsilon}$) ($\bigtriangledown$) and negative heats of mixing ($\epsilon_{AB} = 1.1\bar{\epsilon}$) ($\bigtriangleup$) with $\sigma_{AB} = \bar{\sigma}$ and for bond shortening $\sigma_{AB} = 0.99\bar{\sigma}$ with $\Delta H_{\rm mix} = 0$ ($\diamond$). (Inset) Cohesive energy ratio $\epsilon_{BB}/\epsilon_{AA}$ versus the atomic size ratio σ_{BB}/σ_{AA} for common binary metallic glass formers.[5]

for the two components for most binary bulk metallic glass formers. In Fig. 5, we show R_c as a function of $\epsilon_{BB}/\epsilon_{AA}$ for binary LJ mixtures with $N = 1372$ at fixed $f_B = 0.5$, $(\epsilon_{AA} + \epsilon_{BB})/2 = 1$, and heat of mixing $\Delta H_{\rm mix} = 0$, assuming $\Delta H_{\rm mix} = (\epsilon_{AA} + \epsilon_{BB})/2 - \epsilon_{AB}$[32–34] and the mixing rules $\epsilon_{AB} = (\epsilon_{AA} + \epsilon_{BB})/2$ and $\sigma_{AB} = (\sigma_{AA} + \sigma_{BB})/2$. We find that the glass-forming ability increases (i.e., R_c decreases) as $\epsilon_{BB}/\epsilon_{AA}$ decreases below 1. This result is consistent with the fact that most binary glass formers with $0.8 < \alpha < 1$ possess $\epsilon_{BB}/\epsilon_{AA} < 1$.[5] (See the inset to Fig. 5.)

Inoue's guidelines[2] suggest that a negative heat of mixing $\Delta H_{\rm mix} < 0$ enhances the glass-forming ability of BMGs. The rationale is that a negative heat of mixing makes the mixed and geometrically frustrated state energetically favorable compared to the phase separated state. Figure 1 (right) shows that $\Delta H_{\rm mix}$ is approximately 5%-10% of the average cohesive energy of the two components, $(\epsilon_{AA} + \epsilon_{BB})/2$, for most binary BMGs.[4,5,35] However, we show in Fig. 5 that binary LJ mixtures with heats of mixing in the range $2\Delta H_{\rm mix}/(\epsilon_{AA} + \epsilon_{BB}) = \pm 0.1$ possess the same critical cooling rate R_c as those with $\Delta H_{\rm mix} = 0$ over the full range of size ratios studied.

Why then do most BMGs possess $\Delta H_{\rm mix} < 0$? One possibility is that negative heats of mixing are correlated with strong bonding between atomic species, which can be modeled as bond shortening ($\sigma_{AB} < (\sigma_{AA} + \sigma_{BB})/2$).[36–38] In Fig. 5, we show that only a 1% bond shortening, $\sigma_{AB} = 0.99(\sigma_{AA} + \sigma_{BB})/2$, can give rise to a finite decrease in the critical cooling rate R_c.

IV. CONCLUSION

The glass formability of bulk metallic glass-forming alloys can be characterized by the critical cooling rate R_c, below which the system possesses crystalline domains. The best bulk metallic glasses are those with the lowest values for R_c. However, the key parameters that determine R_c are not currently known, and thus BMGs are mainly developed through a trial and error process. As a first step in computational design of BMGs, we performed molecular dynamics simulations of coarse-grained models for BMGs, binary Lennard-Jones mixtures, and measured R_c as a function of the number fraction, size ratio, relative cohesive energy, and heat of mixing of the two atomic species. We measured the local bond orientational order parameter to quantify the degree of crystallization that had occurred in systems during thermal quenches (at constant volume) from high to low temperature over more than four orders of magnitude in the cooling rate. It is known that weakly polydisperse LJ systems are poor glass-formers; we quantified this statement by showing that the critical cooling rate decreases exponentially with increasing particle size ratio α, $R_c \sim \exp[-C(1-\alpha)^3]$. Further, at a given size ratio $\alpha < 1$, the minimum critical cooling rate occurs at the number fraction corresponding to equal volumes of the large and small particles of equal mass. In addition, we find that at fixed number fraction and size ratio, the critical cooling rate decreases strongly with decreasing cohesive energy ratio of the small particles relative to the large ones, $\epsilon_{BB}/\epsilon_{AA}$. This result may explain why most experimentally obtained binary BMGs possess $\epsilon_{BB}/\epsilon_{AA} < 1$. In contrast, variations of the heat of mixing of the two species in the experimentally accessible range (several percent of the average cohesive energy) do not affect R_c for binary LJ mixtures significantly. However, bond shortening of only several percent relative to $\sigma_{AB} = (\sigma_{AA} + \sigma_{BB})/2$[36–38] does give rise to significant changes in R_c. Recent experiments have suggested that negative heats of mixing are correlated with bond-shortening, which may explain why most experimentally obtained BMGs possess negative heats of mixing. Note that these results come with the caveat that the cooling rates accessible to our MD simulation studies are still several orders of magnitude larger than those used to prepare BMGs in experiments. In future studies, we will characterize the glass-forming ability and crystallization processes in ternary and quaternary LJ mixtures using MD simulations, energy minimization, and genetic algorithms.

ACKNOWLEDGMENTS

We thank Frans Spaepen and Michael Falk for helpful discussions. The authors acknowledge primary financial support from the National Science Foundation (NSF) MRSEC DMR-1119826 (K.Z. and M.W.) and partial support from NSF Grant Nos. DMR-1006537 (C.S.O.) and CBET-0968013 (M.D.S.).

APPENDIX A: THERMOSTAT AND QUENCHING PROTOCOL

In this appendix, we provide additional details of the MD simulations used to thermally quench LJ systems from high temperature liquids to low temperature glasses. The LJ liquids were first equilibrated at high temperature $T_0 = 2.0$ using constant number N, volume V, and temperature T MD simulations, and cooled exponentially $T(t) = T_0 e^{-Rt}$ to low temperature $T_f = 10^{-2}$. The temperature was controlled using

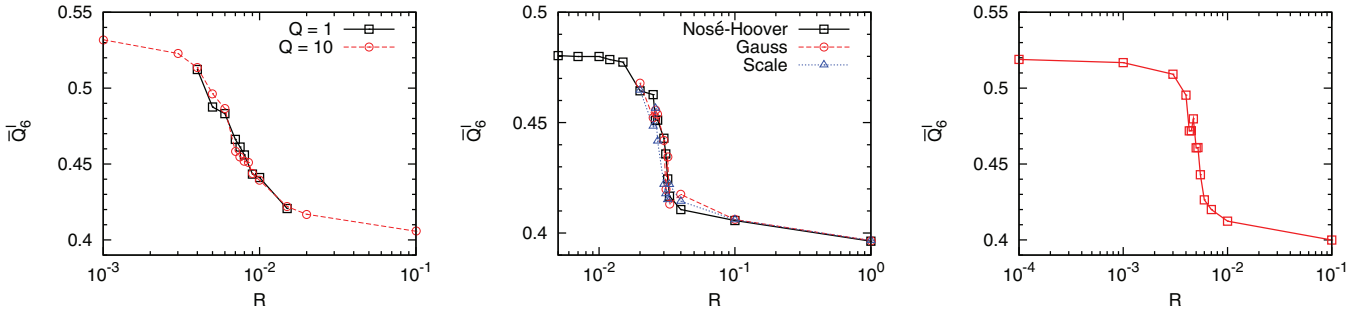

FIG. 6. (Left) Median local bond-orientational order parameter $\overline{Q}_6^l$ versus the cooling rate R for monodisperse LJ systems with $N = 4000$ using the Nosé-Hoover thermostat with thermal inertia parameter $Q = 1$ (□) and 10 (⊙) in units of $m\sigma_{AA}^2$. (Middle) Median local bond-orientational order parameter $\overline{Q}_6^l$ versus R for monodisperse LJ systems with $N = 500$ using several thermostats: Nosé-Hoover (□), Gaussian constraint (⊙), and *ad hoc* velocity rescaling (△). (Right) Median local bond-orientational order parameter $\overline{Q}_6^l$ versus the cooling rate R for monodisperse systems with $N = 1372$ for a linear thermal quenching protocol, $T(t) = T_0 - Rt$, using the Nosé-Hoover thermostat. In each panel, the systems were cooled at constant volume with $\rho = 1$.

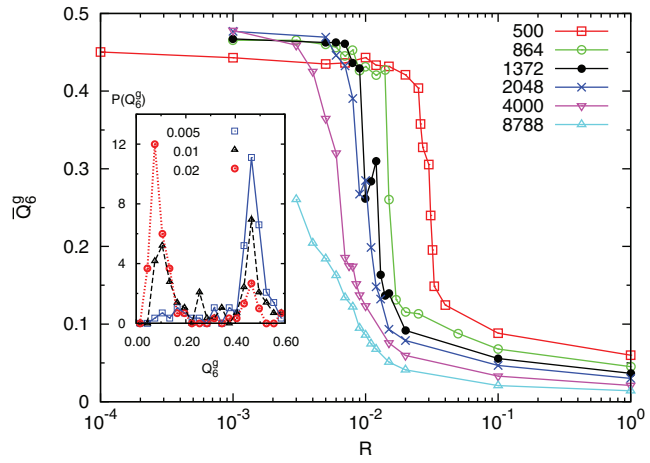

FIG. 7. Median global bond orientational order parameter $\overline{Q}_6^g$ for monodisperse LJ systems following thermal quenches (at constant volume with $\rho = 1$) to $T_f = 0.01$ over a range of cooling rates R for system sizes $N = 500$, 864, 1372, 2048, 4000, and 8788. (Inset) The probability distribution $P(Q_6^g)$ for monodisperse LJ systems with $N = 1372$ following quenches to $T_f = 0.01$ for cooling rates $R = 0.02$ (○), 0.01 (△), and 0.005 (□).

the Nosé-Hoover thermostat[19,20] with thermal inertia parameter $Q = 1$, and the equations of motion were integrated using a Newton's method technique[39] with time step $\Delta t = 10^{-3}$. In Fig. 6 (left), we show for monodisperse LJ systems with $N = 4000$ that the dependence of the median local bond orientational parameter $\overline{Q}_6^l$ on rate R is the same for $Q = 1$ and 10.

We also investigated the extent to which the thermostat affects the critical cooling rate, below which the systems crystallize. In Fig. 6 (center), we show that $\overline{Q}_6^l$ versus R is the same for monodisperse LJ systems with $N = 500$ when the temperature is controlled using the Nosé-Hoover, Gaussian constraint, and *ad hoc* velocity rescaling thermostats.[17,40] Thus, the choice of the thermostat does not influence the measurement of R_c. We also varied the form of the thermal quenching protocol. In Fig. 6 (right), we show that a linear cooling schedule, $T(t) = T_0 - Rt$, gives qualitatively the same results for $\overline{Q}_6^l$ versus R as an exponential temperature ramp.

APPENDIX B: CHARACTERIZATION OF CRYSTALLINE ORDER

In this appendix, we describe several metrics (in addition to the local bond orientational order parameter Q_6^l in

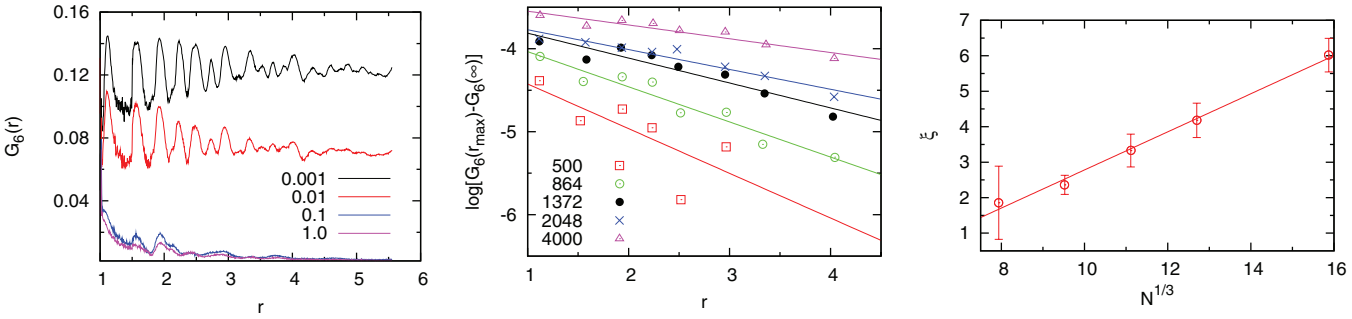

FIG. 8. (Left) Local bond orientational order correlation function $G_6(r)$ for monodisperse LJ systems with $N = 1372$ at several cooling rates $R = 1$, 10^{-1}, 10^{-2}, and 10^{-3} (at constant volume with $\rho = 1$). (Middle) The decay of the local maxima in $G_6(r)$ versus distance r for monodisperse LJ systems at cooling rate $R = 10^{-3}$ (at constant volume with $\rho = 1$) for several system sizes $N = 500$, 864, 1372, 2048, and 4000. (Right) Correlation length ξ from the decay of the local bond orientational order correlation function versus the linear dimension of the system $N^{1/3}$ for monodisperse LJ systems at cooling rate $R = 10^{-3}$. The solid line has slope ≈0.5.

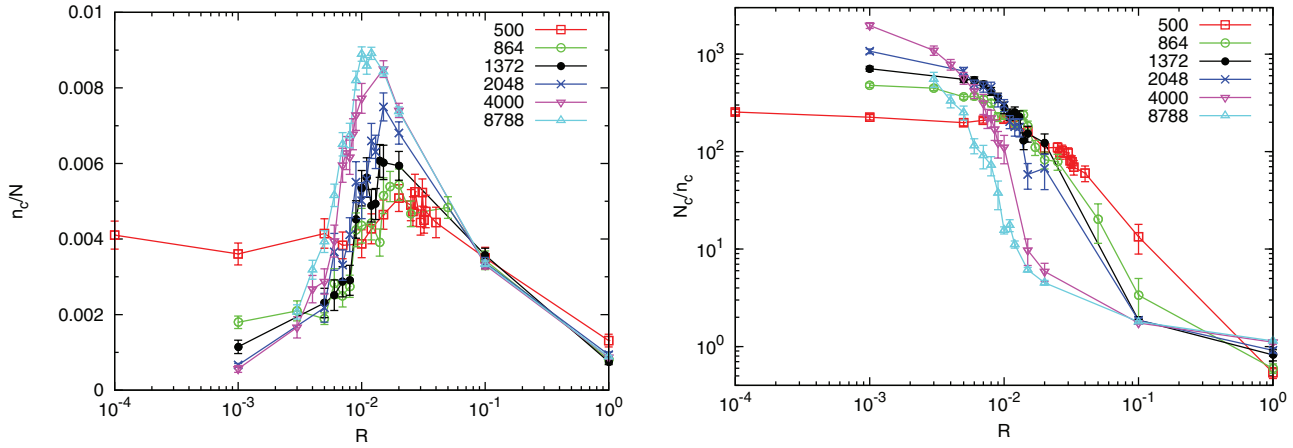

FIG. 9. (Left) The number of crystalline clusters n_c (FCC, HCP, and BCC) normalized by the system size N for monodisperse LJ systems as a function of cooling rate R for several system sizes. (Right) The number of (FCC, HCP, and BCC) crystal-like particles N_c normalized by the number of crystalline clusters n_c (i.e., average crystalline cluster size) as a function of cooling rate for several system sizes. In both panels, the systems were cooled at constant volume with $\rho = 1$.

Eq. (2)) to characterize the degree of crystalline order of thermally quenched LJ systems. In contrast to Q_6^l, the global bond orientational order parameter Q_6^g in Eq. (3) quantifies the degree of crystallization over the entire system. The median global bond orientational order parameter $\overline{Q}_6^g$ versus cooling rate R for monodisperse LJ systems for several system sizes is shown in Fig. 7. $\overline{Q}_6^g$ shows a rapid increase near the critical cooling rate R_c as found for $\overline{Q}_6^l$. However, R_c (defined by a threshold such as $\overline{Q}_6^g = 0.3$) appears to decrease to zero in the large system limit. This trend occurs because it takes an increasing amount of time (and thus slower cooling rates) for crystal nuclei to grow and for the system to reach the same $\overline{Q}_6^g$ as that obtained in smaller systems.

In Fig. 8 (left), we show the local bond orientational order correlation function (Eq. (4)) for monodisperse LJ systems with $N = 1372$ for several cooling rates (at constant volume with $\rho = 1$). We find that $G_6(r)$ plateaus at large r and the plateau value $G_6(\infty)$ increases with decreasing cooling rate R. For partially crystalline systems, $G_6(r)$ decays to $1/\sqrt{N_d}$ at large distances, where N_d is the number of independent crystalline domains. For disordered systems, $G_6(r)$ decays to $1/\sqrt{N_b}$, where N_b is the total number of nearest neighbor particles.[25] We find that the deviation $G_6(r_{\max}) - G_6(\infty)$, where $G_6(r_{\max})$ are the local maxima in $G_6(r)$, decays exponentially $\sim e^{-r/\xi}$ with correlation length ξ. (See Fig. 8.) The correlation length ξ grows linearly with the linear size of the system $N^{1/3}$ for cooling rates $R < R_c$.

We also employed a crystal analysis algorithm to identify the crystalline clusters (FCC, HCP,[27,28,42] or BCC) that form during the thermal quenching process. For slow cooling rates, the system forms only a few large crystalline clusters whose size scales with the system size (see Fig. 9). For fast cooling rates, the number of crystalline clusters is small, and each cluster contains only a few particles. At intermediate rates, the number of crystalline clusters reaches a maximum at a characteristic cooling rate that scales with N as shown in Fig. 9. These results are consistent with the fact that the critical cooling rate R_c (defined using the local bond orientational order parameter Q_6^l) becomes independent of the system size in the $N \to \infty$ limit.

APPENDIX C: THERMAL QUENCHES AT CONSTANT PRESSURE

While constant volume simulations are widely used to study glass formation,[8,9,16] experimental BMGs are commonly processed at constant pressure. We thus also performed thermal quenches to $T_f = 0.01$ in monodisperse LJ systems at constant pressure over a range in pressure from $p = 0.3$ to $p \approx 16$, which corresponds to the largest pressure in the constant volume simulations (where p is expressed in units of $\epsilon_{AA}/\sigma_{AA}^3$), to determine whether our results are sensitive to the choice of the ensemble. Constant pressure was maintained using the Gaussian constraint method.[17] We show in Fig. 10 that for all pressures, the median local bond orientational order parameter $\overline{Q}_6^l$ increases strongly near the critical

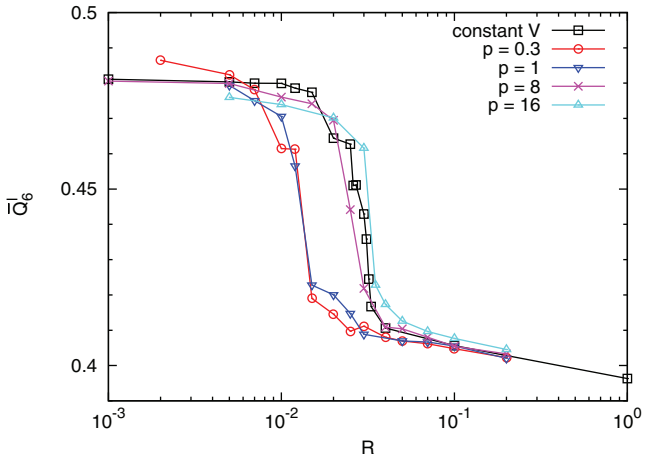

FIG. 10. Median local bond-orientational order parameter $\overline{Q}_6^l$ versus the cooling rate R for monodisperse LJ systems with $N = 500$ obtained by cooling at constant pressure $p = 0.3$, 1, 8, and 16 compared to that for cooling at constant volume with $\rho = 1$.

cooling rate R_c, which decreases with pressure converging to $R_c^0 \approx 10^{-2}$ at low pressure. This result is consistent with previous studies which showed that glass formation phenomenology is similar for the constant volume and constant pressure ensembles.[41]

[1] G. Kumar, P. Neibecker, Y. H. Liu, and J. Schroers, Nat. Commun. **4**, 1536 (2013).
[2] A. Inoue, Acta Mater. **48**, 279 (2000).
[3] D. Turnbull, Contemp. Phys. **10**, 473 (1969).
[4] A. Takeuchi and A. Inoue, Mater. Trans. **46**, 2817 (2005).
[5] D. B. Miracle, W. S. Sanders, and O. N. Senkov, Philos. Mag. **83**, 2409 (2003).
[6] P. Jalali and M. Li, Intermetallics **12**, 1167 (2004).
[7] P. Jalali and M. Li, Phys. Rev. B **71**, 014206 (2005).
[8] W. Kob and H. C. Andersen, Phys. Rev. E **51**, 4626 (1995).
[9] W. Kob, C. Donati, S. J. Plimpton, P. H. Poole, and S. C. Glotzer, Phys. Rev. Lett. **79**, 2827 (1997).
[10] S. Sastry, P. G. Debenedetti, and F. H. Stillinger, Nature **393**, 554 (1998).
[11] W. Kob and J. Barrat, Phys. Rev. Lett. **78**, 4581 (1997).
[12] M. Utz, P. G. Debenedetii, and F. H. Stillinger, Phys. Rev. Lett. **84**, 1471 (2000).
[13] K. Vollmayr, W. Kob, and K. Binder, J. Chem. Phys. **105**, 4714 (1996).
[14] A. Widmer-Cooper, H. Perry, P. Harrowell, and D. R. Reichman, Nat. Phys. **4**, 711 (2008).
[15] S. C. Glotzer, J. Non-Cryst. Solids **274**, 342 (2000).
[16] S. Singh, M. D. Ediger, and J. J. de Pablo, Nature Mater. **12**, 139 (2013).
[17] M. P. Allen and D. J. Tildesley, *Computer Simulation of Liquids* (Oxford University Press, New York, 1987).
[18] A. B. Hopkins, Y. Jiao, F. H. Stillinger, and S. Torquato, Phys. Rev. Lett. **107**, 125501 (2011).
[19] S. Nose, J. Chem. Phys. **81**, 511 (1984).
[20] W. G. Hoover, Phys. Rev. A **31**, 1695 (1985).
[21] S. Zhen and G. J. Davies, Phys. Status Solidi A **78**, 595 (1983).
[22] P. J. Steinhardt, D. R. Nelson, and M. Ronchetti, Phys. Rev. B **28**, 784 (1983).
[23] M. D. Rintoul and S. Torquato, J. Chem. Phys. **105**, 9258 (1996).
[24] T. M. Truskett, S. Torquato, and P. G. Debenedetii, Phys. Rev. E **62**, 993 (2000).
[25] C. F. Schreck, and C. S. O'Hern, in *Experimental and Computational Techniques in Soft Condensed Matter Physics*, edited by J. Olafsen (Cambridge University Press, Cambridge, 2010), pp. 25–61.
[26] Y. T. Wang, S. Teitel, and C. Dellago, J. Chem. Phys. **122**, 214722 (2005).
[27] A. Stukowski, Modell. Simul. Mater. Sci. Eng. **20**, 045021 (2012).
[28] HCP-like particles and clusters reported in this work are identified by considering the first nearest neighbors of each particle. If instead, the superlattice across stacking layers was included, most of the HCP clusters would be classified as "9R" structures[42] (with repeating motifs composed of an FCC layer followed by two HCP layers).
[29] M. D. Rintoul and S. Torquato, Phys. Rev. Lett. **77**, 4198 (1996).
[30] J. D. Honeycutt and H. C. Andersen, Chem. Phys. Lett. **108**, 535 (1984).
[31] J. D. Honeycutt and H. C. Andersen, J. Phys. Chem. **90**, 1585 (1986).
[32] A. R. Miedema, R. Boom, and F. R. Deboer, J. Less-Common Met. **41**, 283 (1975).
[33] R. Boom, F. R. de Boer, and A. R. Miedema, J. Less-Common Met. **45**, 237 (1976).
[34] R. Boom, F. R. de Boer, and A. R. Miedema, J. Less-Common Met. **46**, 271 (1976).
[35] J. H. O. Varley, Philos. Mag. **45**, 887 (1954).
[36] Y. Q. Cheng, E. Ma, and H. W. Sheng, Phys. Rev. Lett. **102**, 245501 (2009).
[37] X. J. Liu, X. D. Hui, G. L. Chen, and T. Liu, Phys. Lett. A **373**, 2488 (2009).
[38] O. N. Senkov, Y. Q. Cheng, D. B. Miracle, E. R. Barney, A. C. Hannon, and C. F. Woodward, J. Appl. Phys. **111**, 123515 (2012).
[39] D. Frenkel and B. Smit, *Understanding Molecular Simulation* (Academic Press, 2002).
[40] D. Brown and J. H. R. Clarke, Mol. Phys. **51**, 1243 (1984).
[41] D. M. Colucci, G. B. McKenna, J. J. Filliben, A. Lee, D. B. Curliss, K. B. Bowman, and J. D. Russell, J. Polym. Sci. **35**, 1561 (1997).
[42] F. Ernst, M. W. Finnis, D. Hofmann, T. Muschik, U. Schönberger, and U. Wolf, Phys. Rev. Lett. **69**, 620 (1992).